Research Square

Preprints are preliminary reports that have not undergone peer review. They should not be considered conclusive, used to inform clinical practice, or referenced by the media as validated information.

Breaking the Equilibrium Yield Limit of Methane Aromatization Using Tandem Chemical Looping Catalysis

Fanxing Li

fli5@ncsu.edu

North Carolina State University https://orcid.org/0000-0002-6757-1874

Ibrahim Sultan

North Carolina State University

Baitang Jin

North Carolina State University

Zhenhua Xie

Columbia University https://orcid.org/0000-0003-3737-8894

Md Emdadul Haque

West Virginia University https://orcid.org/0000-0002-0808-2755

Ashley Caiola

West Virginia University

Jianli Hu

West Virginia University

Debangsu Bhattacharyya

West Virginia University https://orcid.org/0000-0001-9957-7528

Luke Neal

North Carolina State University

Jingguang Chen

Columbia University

Article

Keywords: oxidative coupling, dehydroaromatization, chemical looping, tandem catalysis

Posted Date: November 6th, 2026

DOI: https://doi.org/10.21203/rs.3.rs-11543352/v1

License: This work is licensed under a Creative Commons Attribution 4.0 International License.
Read Full License

Additional Declarations: Yes there is potential Competing Interest. This work was supported in part by the US Department of Energy (DE-FE0032507). The prime recipient of this support is Redox and Catalytic Solutions, LLC, an NC State University-based startup company with Fanxing Li and Luke Neal as co-founders.

Breaking the Equilibrium Yield Limit of Methane Aromatization Using Tandem Chemical Looping Catalysis

Ibrahim Sultan[a,#], Baitang Jin[a,#], Zhenhua Xie[b,c], Md Emdadul Haque[d], Ashley Caiola[d], Jianli Hu[d], Debangsu Bhattacharyya[d], Luke Neal[a], Jingguang G. Chen[b,c,*], Fanxing Li[a,*]

[a] *Department of Chemical and Biomolecular Engineering, North Carolina State University, 911 Partners Way, Raleigh, NC 27695, USA;*

[b] *Department of Chemical Engineering, Columbia University, New York, NY 10027, USA;*

[c] *Chemistry Division, Brookhaven National Laboratory, Upton, NY 11973, USA;*

[d] *Department of Chemical and Biomedical Engineering, West Virginia University, Morgantown, WV 26506, USA*

[#] *These authors contributed equally*

[*] *Corresponding authors: fli5@ncsu.edu (F.L.); jgchen@columbia.edu (J.G.C.)*

Abstract

The direct conversion of methane to aromatics offers a promising route for liquefying natural gas and biogas, thereby generating higher-value chemicals and reducing transportation costs. However, conventional methane dehydroaromatization (MDA) is severely hindered by thermodynamic limitations, high temperature requirements, and catalyst instability. Here, we report a tandem chemical looping catalysis strategy that integrates chemical looping oxidative coupling of methane (CL-OCM) with dehydroaromatization (DHA), overcoming these challenges. The CL-OCM route generates more readily convertible C_{2+} intermediates while consuming hydrogen, the equilibrium-limiting byproduct, as water. This shifts the equilibrium and renders the overall reaction exothermic, achieving a single-pass aromatic yield of 27.1%, 2.5 to 3 times the single-pass yields of conventional MDA. Independent regeneration of the two catalyst beds maintains stable performance over repeated reaction-regeneration cycles. Process analysis projects ~75% lower levelized costs and ~77% lower cradle-to-gate emissions than direct MDA.

Keywords: oxidative coupling, dehydroaromatization, chemical looping, tandem catalysis

Introduction

Methane is an abundant carbon resource in natural gas and biogas, yet much of it remains underutilized or flared when such resources are remote, small-scale or compositionally variable.[1–7] Converting methane directly into transportable liquid hydrocarbons would create an intensified alternative to conventional syngas-based gas-to-liquids routes, which require extensive process steps such as reforming, gas conditioning, synthesis, refining, and separations. The primary challenge to direct methane conversion to non-syngas products is its

high stability relative to the target products.[8–11] As such, direct routes must activate strong C-H bonds while avoiding overoxidation or carbon deposition.

Direct methane dehydroaromatization (MDA) is one of the most attractive routes because it converts methane to benzene and related aromatic hydrocarbons without first forming syngas.[2,12,13] However, conventional MDA remains limited by a combination of unfavorable thermodynamics, high thermal energy demand, and rapid catalyst deactivation.[14] The coproduct H_2 restricts methane conversion and aromatic yield (~12% equilibrium benzene yield at 700 °C), while the strongly endothermic reaction ($6CH_4 = 9H_2 + C_6H_6\,\Delta H_r^o = +531\,\mathrm{kJ/mol}$) requires substantial high-temperature heat input. As a result, single-pass aromatic yields in direct MDA are typically low (≤10% in experimental studies), despite decades of catalyst development.[15,16] Meanwhile, metal-modified zeolite catalysts tend to deactivate rapidly through coke formation and restructuring under the severe MDA reaction environment.[15,16]

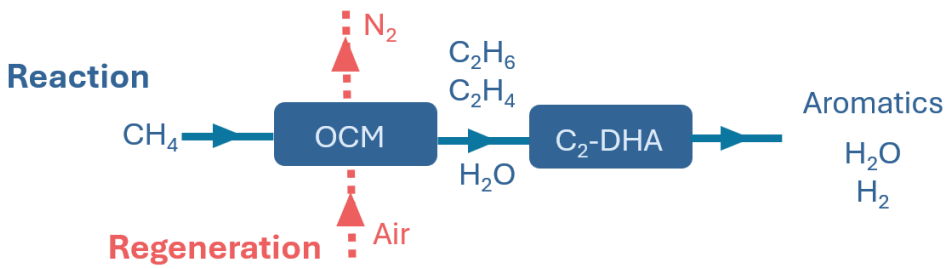
Efforts to overcome these limitations have largely focused on removing or consuming H_2. Membrane reactors with staged oxygen co-feeding,[17] electrochemical oxygen pumping,[18] downstream selective H_2 combustion via chemical looping,[19,20] and *in situ* H_2 scavengers[21] have each improved aspects of the reaction. Nevertheless, these strategies still rely on direct MDA as the core reaction chemistry and only partially address the coupled limitations of equilibrium, heat input and catalyst stability. Some approaches also introduce additional process complexity. Direct coupling of an oxidative coupling of methane (OCM) effluent to a conventional Mo/ZSM-5 MDA catalyst has also been reported, but it gave only ~2.5% benzene yield at 14% methane conversion, with CO_2 in the effluent oxidizing the Mo_2C active phase.[22] Simply placing an aromatization bed downstream of OCM is therefore insufficient to improve the MDA performance.

In this study, we report a tandem chemical looping strategy that redirects methane aromatization to a more favorable C_2-mediated pathway. Methane is first converted to ethylene- and ethane-rich C_{2+} intermediates through chemical looping - oxidative coupling of methane (CL-OCM),[23] and these intermediates are subsequently converted to aromatics over a downstream dehydroaromatization (DHA) catalyst. This architecture synergistically combines an exothermic methane-coupling step with aromatization of more reactive C_{2+} intermediates, creating a reaction network that can circumvent the equilibrium and endothermicity constraints of direct MDA. We show that the key upstream catalyst requirement is not simply high total C_{2+} yield, but the right combination of C_{2+} yield and ethylene-rich product distribution. Integrating this catalyst-design principle with independently controlled redox regeneration gives a single-pass aromatic yield of 27.1%, roughly 2.5–3 times that of conventional MDA. Repeatable cyclic operation was also demonstrated. Process analysis further indicates that the tandem scheme can operate autothermally and convert distributed methane to aromatics with a cradle-to-gate carbon footprint about 77% lower than that of direct MDA when low-carbon electricity is used.

Results

Tandem reaction design enables high-yield and overall exothermic methane aromatization

a



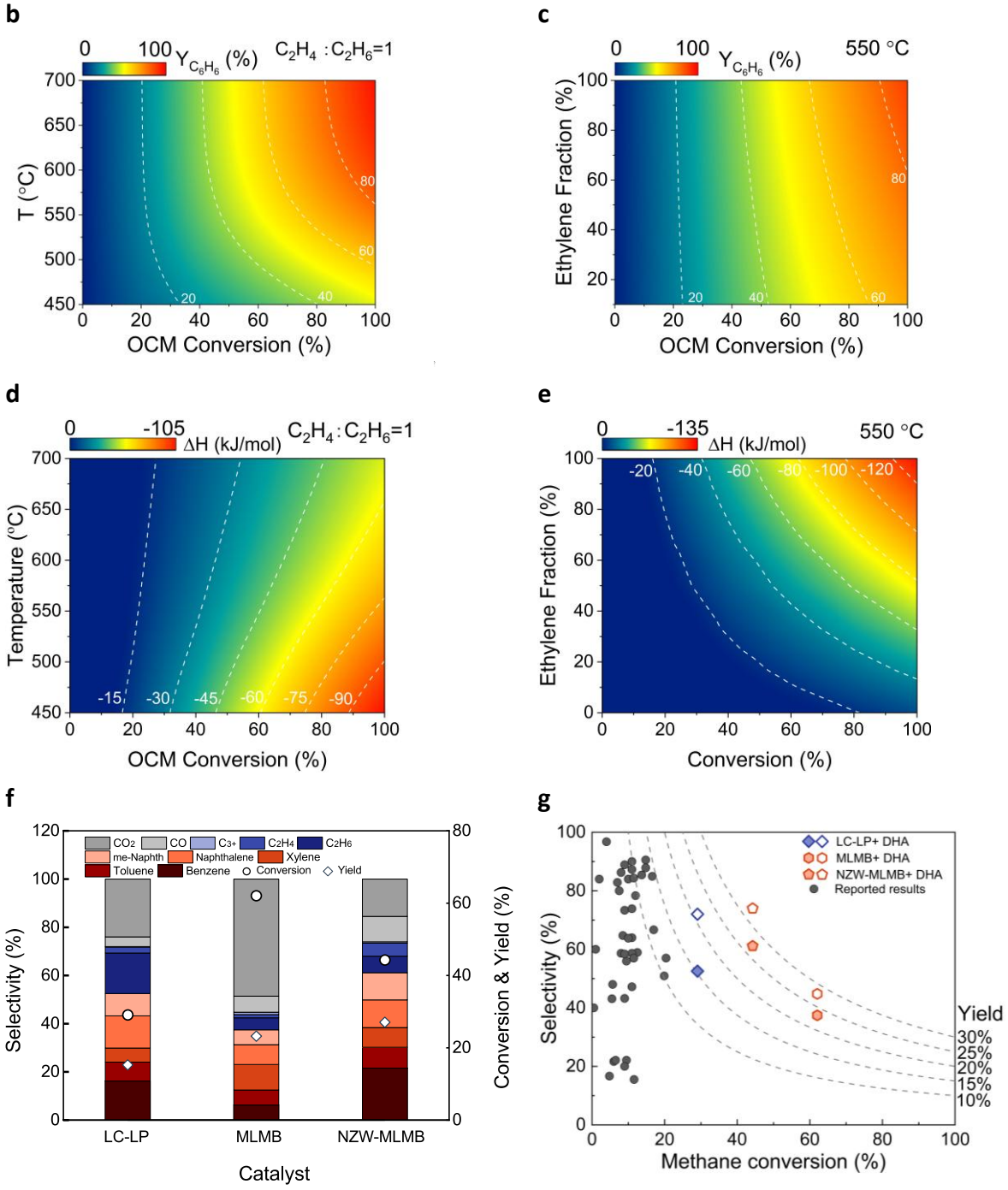


Figure 1. Thermodynamic design and experimental realization of tandem chemical looping methane aromatization. **a.** Tandem chemical looping reaction architecture for C_2-mediated methane aromatization; **b.** Equilibrium benzene yield versus the DHA step temperature and OCM conversion (under a fixed C_2H_4:C_2H_6 of 1); **c.** Equilibrium yield as a function of OCM conversion and ethylene fraction with the DHA step at 550 °C; **d/e.** Overall reaction enthalpy over the same design space as b and c, respectively; **f.** Performance of tandem chemical looping

OCM-DHA for different CL-OCM redox-oxide formulations with DHA catalyst (LC-LP: Li_2CO_3-modified $LaPrO_x$ at 725 °C; MLMB and NZW-MLMB at 840 °C; HGaAlMFI at 550 °C in all cases; full conditions provided in Table S1); g. Comparisons of the OCM-DHA performance in the current study with literature reported MDA performance. Filled symbols correspond to aromatics selectivities whereas unfilled symbols correspond to total C_{2+} selectivities from methane conversion.

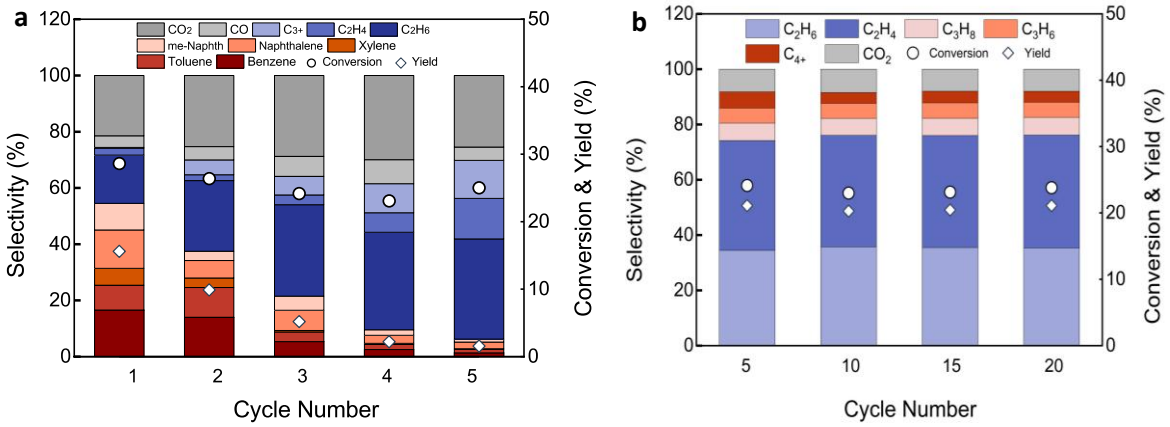
Direct MDA must activate methane, form C–C bonds and aromatize within a single, strongly endothermic and equilibrium-limited reaction. We instead split the chemistry into two complementary stages (Fig. 1a): chemical looping oxidative coupling of methane (CL-OCM) converts methane into ethylene, ethane and other C_{2+} hydrocarbons using lattice oxygen from a regenerable redox catalyst, and the resulting C_{2+} stream passes over a dehydroaromatization catalyst that converts it into benzene and higher aromatics. Oxidative coupling releases high-grade heat and converts hydrogen into water, and the C_{2+} intermediates, particularly ethylene, aromatize far more favorably than methane.[24] At the OCM conversion demonstrated experimentally (~44%), the equilibrium aromatic yield is roughly three times that of direct MDA, rising to five-fold at higher OCM conversions, with a net heat release of up to ~130 kJ per mol of methane fed (Fig. 1d,e).

At a fixed ethylene fraction, $C_2H_4/(C_2H_4 + C_2H_6)$, the equilibrium benzene yield rises steeply with OCM conversion and stays well above that of direct MDA across the DHA temperature range (Fig. 1b), while the heat released by oxidative coupling more than offsets the heat consumed by aromatization, so the overall sequence is exothermic throughout the experimentally relevant window (Fig. 1d; confirmed by the process simulation presented later). Stream composition adds a second dimension: at 550 °C, a higher ethylene fraction raises both the equilibrium yield and the net heat release (Fig. 1c,e), because ethylene aromatizes more readily, and exothermically, whereas ethane aromatization is endothermic.

We tested this prediction in the two-reactor setup (Fig. S1) using three CL-OCM formulations with distinct C_{2+} yields and ethylene fractions: Li_2CO_3-modified $LaPrO_x$ (LC-LP),[23] Li- and B-promoted Mn–Mg-based redox oxide, $MnLi_aMg_bB_cO_x$ (MLMB),[25] and an MLMB-$NaZrWO_x$[25–27] (NZW-MLMB) composite (Fig. S2). Li_2CO_3-modified $LaPrO_x$ gave a high C_{2+} yield (26.4%) but an ethane-rich stream (ethylene fraction 64.2%); MLMB gave a lower C_{2+} yield (23.1%) with a higher ethylene fraction (78.6%); and adding the $NaZrWO_x$ promoter shifted the distribution further toward ethylene while suppressing non-selective oxidation (C_{2+} yield 32.7%, ethylene fraction 90.5%). Among the DHA candidates screened, HGaAlMFI was the most effective (Fig. S3). Coupled with HGaAlMFI, the tandem aromatic yields followed the combined C_{2+}-yield and ethylene-fraction criterion rather than C_{2+} yield alone (Fig. 1f,g): MLMB, despite a lower C_{2+} yield than Li_2CO_3-modified $LaPrO_x$, gave a higher tandem aromatic yield (23% versus 16%), and MLMB-$NaZrWO_x$, which combines the highest C_{2+} yield with the highest ethylene fraction, gave the highest aromatic yield of approximately 27.1% at a methane conversion of 44.3% (Fig. 1g), more than 2.5 times the single-pass aromatic yields accessible through direct MDA (typically <10%).

DHA catalyst performance, stability, and reactivation of active sites

Steam-induced DHA deactivation motivates independent catalyst regeneration



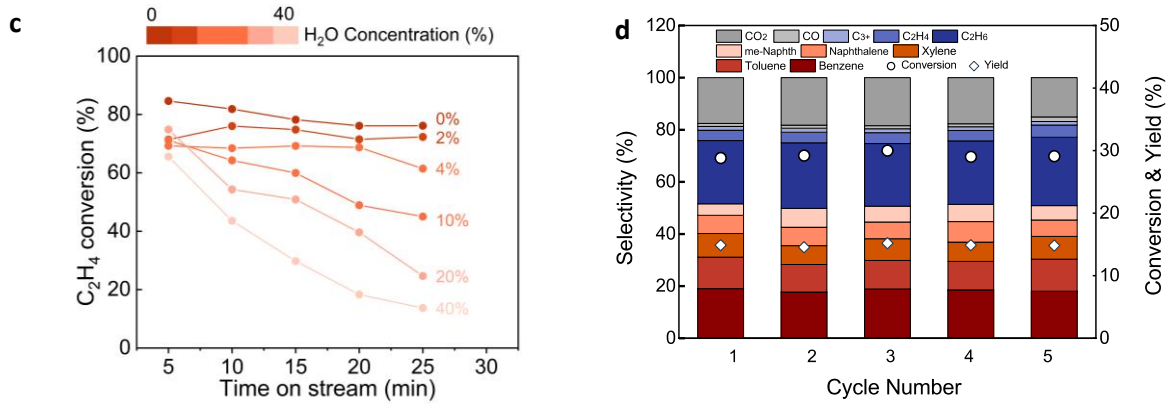


Figure 2. a. Tandem CL-OCM-DHA cycling with O_2 regeneration of both beds, showing rapid loss of aromatic yield. **b.** Standalone CL-OCM cycling, showing that the OCM bed remains comparatively stable. **c.** Effect of H_2O concentration on C_2H_4-DHA over HGaAlMFI. **d.** Tandem CL-OCM-DHA cycling with independent O_2 regeneration of the CL-OCM bed and H_2 regeneration of the DHA bed. Li_2CO_3-modified $LaPrO_x$ (700 °C) and HGaAlMFI (550 °C) were used in a, b and d; conditions for all panels are given in Table S1.

The tandem pathway also creates a stability challenge absent from dry C_{2+} dehydroaromatization. The lattice oxygen that drives methane coupling leaves the CL-OCM effluent with roughly 15–30 vol% steam, so the downstream DHA catalyst receives the desired C_{2+} intermediates together with a strongly deactivating component. We first evaluated the tandem system using the Li_2CO_3-$LaPrO_x$ CL-OCM redox catalyst and a conventional chemical looping regeneration protocol, in which both reactors were purged and then oxidized with 20% O_2 after each methane reaction step. Under these conditions, the first cycle gave an aromatic yield of 15.6% at 28.6% methane conversion. However, the aromatic yield decreased to 9.9% in the second cycle and to 1.6% by the fifth cycle, even though methane conversion decreased more modestly from 28.6% to 24.0% (Fig. 2a). At the same time, the selectivity shifted away from aromatics and toward light hydrocarbons, indicating that the system continued to generate C_{2+} intermediates but progressively lost the ability to convert them into aromatics. Fig. 2b confirms that the CL-OCM catalyst alone retained stable methane conversion and C_{2+} yield

over the same cycling. Therefore, the loss of aromatics originated in the downstream DHA bed rather than in the methane-coupling function.

To isolate the effect of steam, we ran C_2H_4-DHA over HGaAlMFI with controlled H_2O co-feeds (Fig. S4). Water is known to oxidize the reduced Ga species, such as $[GaH_2]^+$, that carry the dehydrogenation function of Ga-zeolites,[13,28] and to deactivate Zn-zeolites by forming $Zn(OH)^+$.[29] Under dry conditions, C_2H_4 conversion was relatively stable over the timescale of the experiment; even small amounts of H_2O accelerated deactivation, and higher steam concentrations caused increasingly rapid loss of conversion (Fig. 2c). C_2H_4-TPSR (Fig. S5) and H_2-TPR (Fig. S6) of fresh and steam-treated HGaAlMFI confirm that steam suppresses intrinsic C_2H_4 activation and alters the reducible Ga sites. Steam is therefore the principal cause of the declining aromatization activity in the tandem system.

These results show that a single oxidative regeneration step is incompatible with stable operation of the tandem process. Oxidation is required to replenish lattice oxygen in the CL-OCM redox catalyst, but the steam-exposed DHA catalyst requires a reducing treatment to restore aromatization activity. We therefore implemented an independently controlled regeneration protocol in which O_2 was supplied to the CL-OCM bed, and H_2 was supplied to the DHA bed during the regeneration step (Fig. S1). This strategy stabilized the product distribution and maintained aromatic yield over five repeated tandem cycles (Fig. 2d), demonstrating the potential efficacy of this approach. The molecular basis for this recoverable DHA deactivation is examined in the following section.

Reversible Ga-site redox enables DHA reactivation

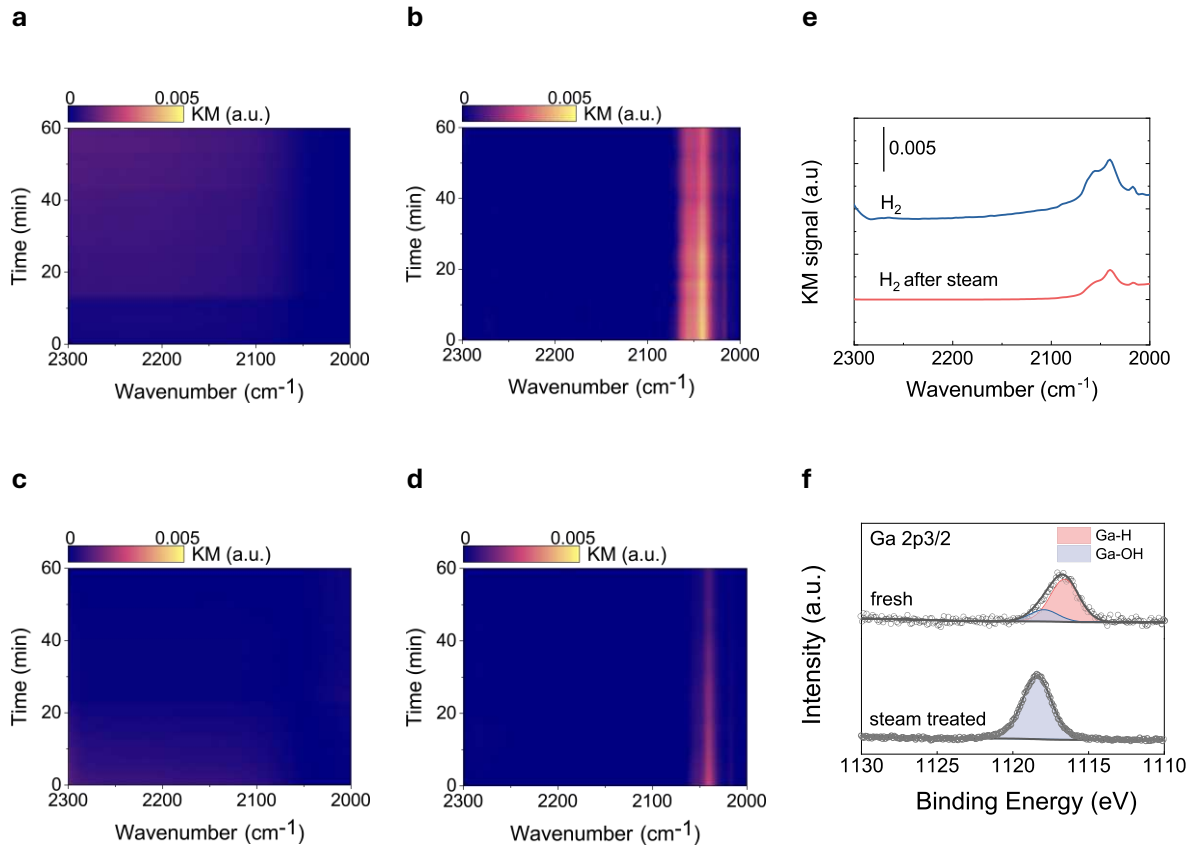


Figure 3. DRIFTS of DHA catalyst after (a) H_2 treatment (300 °C), (b) H_2 treatment (550 °C), (c) H_2 and steam treatment (550 °C), (d) Steam and H_2 treatment (550 °C), (e) Comparison of H_2 treatment and steam-H_2 treatment, (f) XPS of fresh and steam-treated catalysts.

Recovery upon H_2 regeneration implied that the steam-induced deactivation is reversible. We therefore followed the state of Ga in HGaAlMFI under H_2 and H_2O by DRIFTS, XPS and combined *in situ* X-ray absorption spectroscopy (XAS) and X-ray diffraction (XRD), interrogating which species steam consumes and whether reduction regenerates them.

DRIFTS showed that the reduced state of HGaAlMFI forms only under sufficiently high-temperature H_2 treatment (Fig. 3a–e): no hydride feature appeared in the 2000–2100 cm^{-1} region after H_2 at 300 °C, whereas H_2 at 550 °C produced two bands near 2040 and 2057 cm^{-1}

that are assigned, following prior studies of Ga-zeolites,[30,31] to Ga–H species such as $[GaH_2]^+$ and $[GaH]^{2+}$ associated with the dehydrogenation function of Ga-containing zeolites.

Steam exposure strongly attenuated these Ga-H-associated bands. This change is consistent with oxidation or hydroxylation of reduced Ga species by H_2O, converting the catalyst away from the reduced state required for efficient C_{2+} dehydroaromatization. Importantly, the bands reappeared after subsequent H_2 treatment (Fig. 3d,e), although only to roughly half of their original intensity, indicating that the steam-induced change in Ga speciation is largely reversible under the reducing conditions used during DHA-bed regeneration. XPS measurements showed a corresponding shift in the Ga $2p_{3/2}$ from a binding energy (1116.6 eV), which corresponds to Ga-H species, toward one consistent with oxidized gallium species,[32] such as the hydroxide (1118.4 eV) after steam treatment (Fig. 3f), supporting the conclusion that H_2O changes the local chemical environment of Ga rather than merely blocking external surface sites.

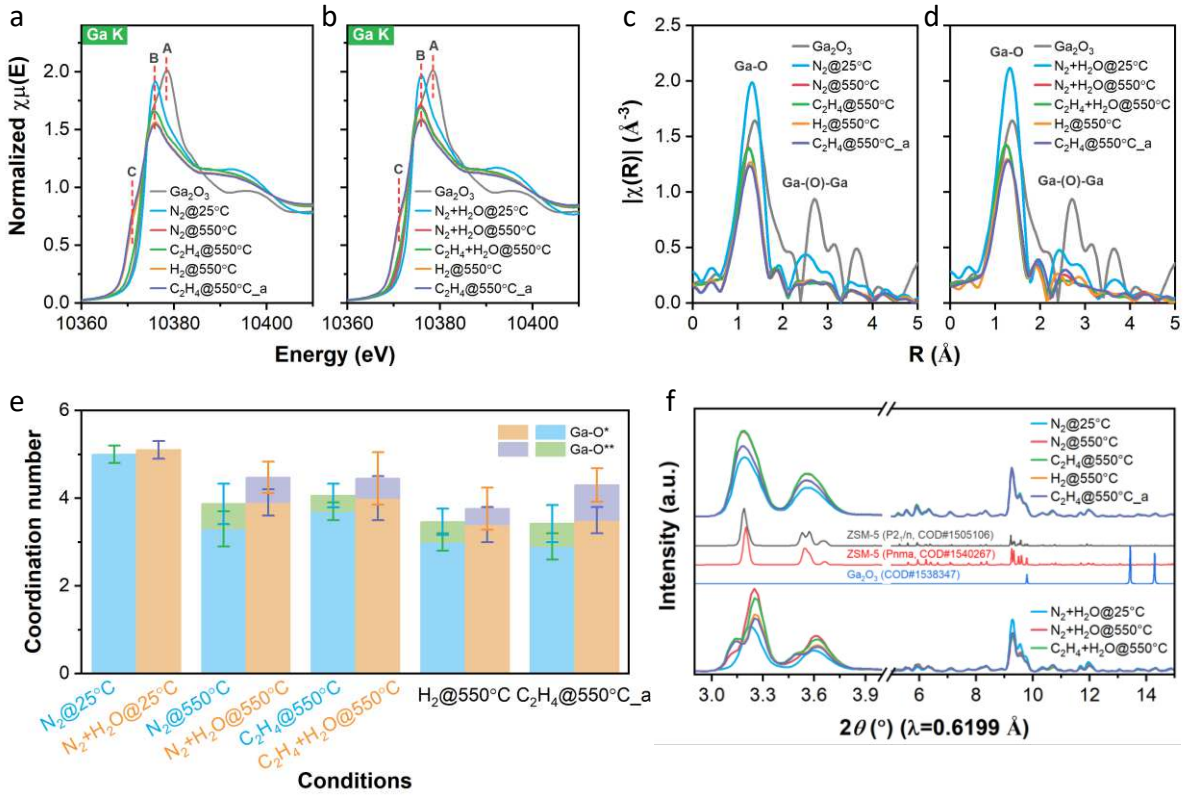


Figure 4. Combined in situ XAS-XRD characterization of the HGaAlMFI catalyst under different conditions. (a) and (b) in situ Ga K-edge XANES plots of HGaAlMFI and Ga_2O_3; (c) and (d) k^2-weighted FT-EXAFS plots in R space of the Ga K-edge; (e) Evolution of coordination numbers of different Ga-O bonds under different conditions; (f) *in situ* XRD patterns of the HGaAlMFI catalyst under different conditions; for clarity, identical conditions in the two XRD series share the same legend, while different conditions are labeled separately in the lower-right corner. Notes: Ga-O* and Ga-O** referred to shorter and longer Ga-O bonds, respectively; N_2 (or C_2H_4)+H_2O indicated that the steam was co-fed with N_2 (or C_2H_4); "C_2H_4@550°C_a" represented running the reaction in C_2H_4 at 550 °C again.

To elucidate the behavior of active sites for the DHA catalyst, changes in the chemical states of Ga, its local coordination and phases under varying pretreatment and reaction conditions were examined using combined *in situ* XAS and XRD techniques (Fig. 4). In the fresh catalyst, XANES shows Ga predominantly in tetrahedral coordination with oxygen, evidenced by the characteristic "peak B" (Fig. 4a) in contrast to the dominant peak A of the Ga_2O_3 reference, and no Ga_2O_3 is detected by EXAFS or XRD (Fig. 4c,f), indicating highly dispersed GaO_x. Heating to 550 °C in N_2 lowers the coordination number of the shorter Ga–O* shell from ~5.0 to ~3.3 and removes the Ga–(O)–Ga contribution characteristic of extra-framework GaO_x (Fig. 4c,e, Table S2), consistent with reduction of extra-framework Ga and its migration into the zeolite pores by exchange with Brønsted protons; Ga–O* and Ga–O** are assigned to intra- and extra-framework Ga–O bonds, respectively.[24] Reaction in C_2H_4 changes the coordination little, but H_2 treatment followed by a second C_2H_4 exposure lowers CN(Ga–O*) further to ~3.0 and produces a new pre-edge feature, peak C (Fig. 4a), attributed to Ga^+ and/or $[Ga(III)H_2]^+$ species, the latter being unstable above 500 °C.[16,33,34] Full fitting results are given in Figs. S7–S9 and Tables S2–S4.

With steam pretreatment, the same sequence gives systematically higher Ga–O coordination numbers (Fig. 4b,d,e and Table S3). Steam has been reported to oxidize Ga^+ species and deactivate the Lewis acid sites, which are difficult to regenerate and impose a high energy penalty (ΔH = 302 kJ mol^{-1}).[28,35,36] Subsequent H_2 treatment again restored the reduced Ga state, but after renewed C_2H_4 exposure a Ga–(O)–Ga contribution reappeared (Fig. 4d) and CN(Ga–O**) rose to ~0.8, indicating formation of GaO_x species not seen under anhydrous conditions (EXAFS details for Ga_2O_3 are given in Fig. S9 and Table S4).

In situ XRD revealed that, under the anhydrous atmosphere at 550 °C (Fig. 4f), the ZSM-5 framework predominantly adopted a *Pnma* symmetry with preserved crystallinity, as suggested by the stable 2θ peaks between $9-10°$, while the steam treatment decreased the ZSM-5 crystallinity.[37,38] Under reaction conditions, shoulder peaks appeared at lower angles than the dominant peaks between 3.0–3.9°, suggesting the incorporation of Ga cations and/or the formation of secondary porosity (e.g., mesopores or structural defects), while the short-range order was preserved. Unlike the change of Ga species, these changes cannot be restored by H_2.

Taken together, steam changes both the Ga speciation and, less reversibly, the zeolite framework. Because H_2 regeneration restores the reduced Ga state and with it the aromatization activity, the Ga speciation is the dominant factor; the residual framework and GaO_x changes are the likely origin of the slow decline seen over extended cycling (Fig. S10). Stable tandem operation therefore needs two regeneration chemistries: the CL-OCM bed must be oxidized to replenish lattice oxygen, and the DHA bed must be reduced to restore the Ga state associated with C_{2+} dehydroaromatization.

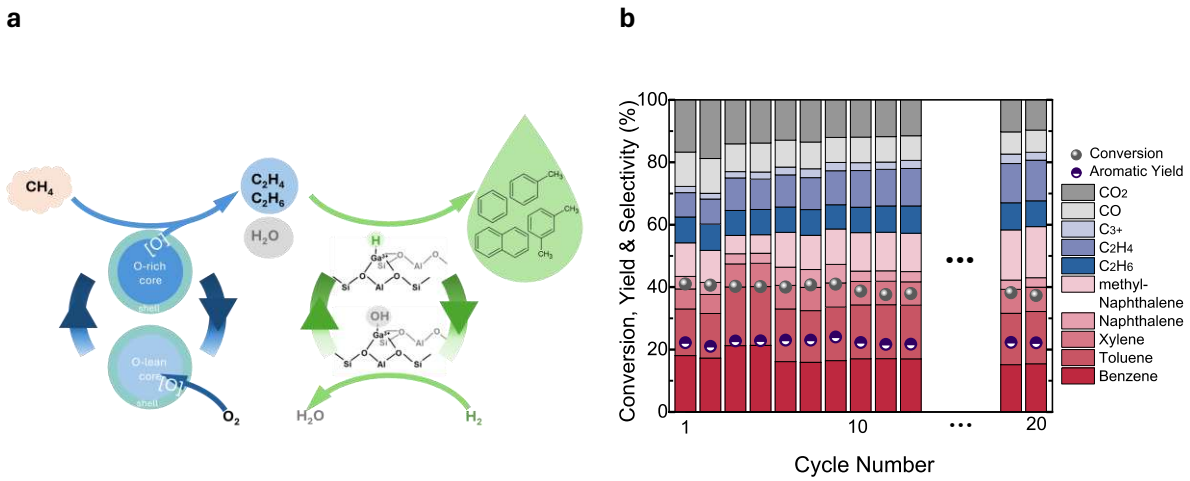


Figure 5. (a) Scheme of the tandem OCM+DHA with chemical looping; (b) Stability of the tandem CL-OCM-DHA system with MLMB-NaZrWO$_x$ (840 °C) and HGaAlMFI (550 °C) over 20 reaction-regeneration cycles under the dual O$_2$/H$_2$ regeneration protocol (detailed conditions in Table S1).

Dual chemical looping sustains high-yield tandem aromatization

We implemented this requirement as a dual chemical looping protocol in which the MLMB-NaZrWO$_x$ CL-OCM bed and the HGaAlMFI DHA bed are regenerated independently after each methane step (Fig. 5a). Methane first contacts MLMB-NaZrWO$_x$ at 840 °C; the ethylene-rich effluent passes directly to HGaAlMFI at 550 °C; the system is purged with Ar; O$_2$ is then fed to the CL-OCM bed while H$_2$ is fed separately to the DHA bed; and a second purge precedes the next methane step.

Using this dual-looping protocol, the MLMB-NaZrWO$_x$/HGaAlMFI tandem system maintained high aromatic yield over 20 reaction-regeneration cycles (Fig. 5b). These cycling experiments were designed to verify the repeatability of the dual-regeneration protocol, as is customary in chemical looping studies, rather than to maximize yield; the operating conditions therefore differ from those of the optimized single-cycle result in Fig. 1f. The aromatic carbon

yield averaged approximately 22.4% and remained above 21.0% throughout the 20-cycle experiment. Methane conversion remained between approximately 37.3% and 41.0%, while aromatic selectivity was approximately 51.8–59.4%. Carbon balances for the reported cycles were within ±10%. This contrasts with the rapid deactivation under oxidative regeneration alone (Fig. 2a): the yield is sustained because MLMB-NaZrWO$_x$ supplies an ethylene-rich feed and the dual-regeneration protocol preserves the downstream aromatization function. Even the sustained ~22% is roughly double the single-pass yields of direct MDA (~10%), and the optimized single-cycle result reaches ~27% (Fig. 1f).

We also evaluated the dual-regeneration strategy with Li_2CO_3-modified LaPrO$_x$ as the upstream CL-OCM catalyst. Although this system produced a lower aromatic yield because of its less favorable C_2 speciation, it operated for 50 reaction-regeneration cycles (~50 h of cyclic operation) with the average aromatic yield remaining above 12.9% (Fig. S10). This supports the broader durability of the independent O_2/H_2 regeneration concept and provides the experimental basis for the process-level analysis that follows.

Process analysis supports techno-economic and sustainability impacts

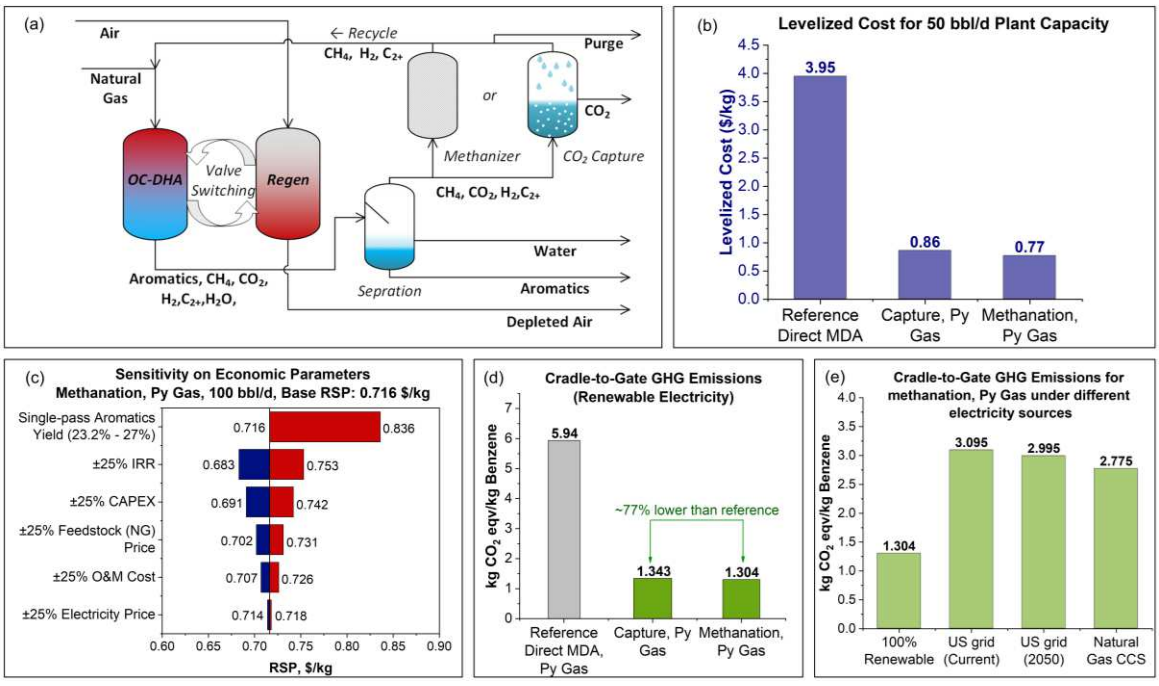


Figure 6. Process-level effects of tandem CL-OCM-DHA: (a) simplified process configurations; (b) economic performance of different process configurations at 50 bbl/d capacity; (c) sensitivity on economic parameters for the methanation case at 100 bbl/d capacity; (d) cradle-to-gate GHG emissions of different process configurations; (e) cradle-to-gate GHG emissions of the methanation case for different electricity sources.

To assess distributed conversion of methane-rich resources into transportable aromatics, we built an Aspen Plus model of a 50 bbl/day organic-liquid plant, a scale commensurate with stranded or underutilized gas (process flow diagrams in Figs. S11–S13 of the Supplementary Information, SI). The reactor section uses the experimentally demonstrated OCM-DHA performance as its design basis. Because the reactor sizing and cost are insensitive to the specific oxygen-carrier formulation, a generic redox-oxide inventory was used in the model (see SI). Methane is converted to a mixture of benzene, toluene, xylenes, naphthalene and related liquids; unconverted methane is recycled, and the CO_2 formed in the redox cycle is handled either by amine-based capture or by methanation and recycle. Two product strategies were compared: complete on-site separation of the individual aromatics, and export of the condensed liquid as a pyrolysis-gasoline-like (Py Gas) stream (Fig. 6a).

The tandem process is projected to cut the levelized cost of aromatics by about three-quarters relative to the scaled reference direct-MDA plant: from 3.95 \$/kg to 0.92–0.98 \$/kg with complete separation and to 0.77–0.86 \$/kg with Py Gas export, the methanation cases being the lower value in each pair (Fig. 6b shows the Py Gas cases; all cases in Table S12 and Fig. S15). At 50 bbl/day the best case falls just short of the 10% target IRR (9.39%); at 100 bbl/day the levelized cost drops to 0.716 \$/kg and the IRR exceeds 10% (Fig. 6c). Capital intensity and financing dominate the sensitivity. Among the economic parameters, single-pass aromatic yield (23.2% to 27.1%) and ±25% changes in IRR and CAPEX produce the largest changes in levelized cost, followed by the natural-gas price, with electricity price having the smallest

effect (Fig. 6c). This is consistent with the low heat burden of the tandem process relative to direct MDA, which reduces its exposure to energy costs.

Life-cycle analysis (LCA) based on the Aspen Plus model (see SI) suggests that the CL-OCM-DHA process can substantially reduce greenhouse-gas emissions relative to the reference direct-MDA process, particularly when low-carbon electricity and carbon management are used. Under a cradle-to-gate boundary and a functional unit of 1 kg benzene-equivalent product, the reference case emitted 5.94 kg CO_2-eq/kg product. In contrast, the CL-OCM-DHA configurations emitted 1.30–1.35 kg CO_2-eq/kg product (~77% lower), with the lowest value obtained for methanation with Py Gas export (Fig. 6d; renewable electricity). The remaining cradle-to-gate emissions were dominated by natural-gas supply, catalyst and equipment materials, and purge losses. The emissions benefit depends strongly on the electricity used. For example, cradle-to-gate, the methanation Py Gas case emissions increase from 1.304 kg CO_2-eq/kg product for renewable electricity to 2.775 kg CO_2-eq/kg with the NG-based electricity with capture system, according to US-DOE's LCA guidelines[39] and 3.095 kg CO_2-eq/kg for current U.S. grid mix electricity (Fig. 6e).

Overall, the process model, TEA, and LCA support that tandem chemical looping goes beyond increasing single-pass methane conversion to potentially enable economic viability at distributed scales, reducing greenhouse-gas emissions relative to direct MDA.

Discussion

This work shows that methane aromatization can be advanced by redesigning the reaction architecture coupled with catalyst innovation and optimizations. Direct MDA asks a single harsh environment to activate methane, form C–C bonds, remove hydrogen, supply heat and keep a zeolite active; tandem chemical looping divides these demands between an exothermic redox coupling step and a downstream aromatization step, and the division brings two design

rules. First, the upstream catalyst is judged not by total C_{2+} yield but by the combination of C_{2+} yield and ethylene fraction, which is why Li_2CO_3-modified $LaPrO_x$, outstanding by the conventional OCM metric, is outperformed by MLMB-$NaZrWO_x$. Second, the two functions must be regenerated under different redox potentials: oxidation restores lattice oxygen upstream, while reduction restores the Ga–H-associated state that steam removes downstream.

Although the cyclic operating mode introduces reactor-switching complexity, it builds on highly successful industrial precedents. CATOFIN and Houdry-type dehydrogenation processes use multiple fixed beds operated out of phase, with beds cycling through reaction, purge or evacuation, air regeneration/reheat and, in many cases, H_2-induced catalyst reduction.[40–42] The tandem CL-OCM-DHA process follows this established logic of cyclic catalytic operation, but applies it to two coupled functions with different regeneration requirements: oxidative regeneration of the upstream redox catalyst and reductive regeneration of the downstream Ga-zeolite. This suggests that practical implementation could proceed through staggered fixed-bed operation, while circulating-fluidized-bed or moving-bed redox reactor concepts may offer alternatives for improved heat transfer and solids handling.[43,44]

At the process level, the CL-OCM step supplies high-temperature heat, the DHA step turns the C_{2+} intermediates into condensable liquids, methane recycle improves carbon utilization, and exporting a mixed aromatic product avoids on-site separation, an important saving at stranded-gas scale, while CO_2 capture or methanation closes the carbon balance. The present TEA and LCA are a first process-level assessment rather than a design: feed impurities, catalyst scale-up and lifetime, purge steps and the multi-reactor operating sequence remain to be engineered, but these are tractable problems with direct precedent in cyclic catalytic reactors.

Overall, tandem chemical looping offers an advanced reaction-engineering strategy for transforming methane aromatization from an equilibrium-limited, endothermic, single-catalyst

problem into a coordinated redox-catalytic process. The broader implication is that chemical looping can do far more than supplying oxygen or removing hydrogen; it can reorganize difficult catalytic transformations into staged reaction networks with more favorable thermodynamics, heat balance and regeneration logic. For methane upgrading, this strategy opens a path toward compact, high-yield and potentially autothermal production of liquid aromatics from distributed gas resources.

AI usage statement

The authors used ChatGPT and Claude during manuscript preparation for language editing and internal mock figure-layout planning. No experimental data, numerical results, scientific conclusions, or publication-ready figures were generated by AI. All AI-assisted content was reviewed, edited, and verified by the authors, who take full responsibility for the final manuscript.

Acknowledgments

This research used beamline 7-BM (QAS) of the National Synchrotron Light Source II (NSLS-II) at BNL (Contract No. DE-SC0012704) and was supported in part by the Synchrotron Catalysis Consortium (Grant No. DE-SC0012653). This research was funded in part by grants from the US Department of Energy, National Energy Technology Laboratory (DE-FE0031869, DE-FE0032507). The authors would like to acknowledge Dr. Xin Li and Prof. Yunfei Gao for their initial contributions to this research. We also thank Prof. Aditya Bhan for helpful discussions.

Author contributions

F.L. conceived the idea and supervised the project. I.S. and B.J. synthesized the catalysts, performed the reactor experiments and DRIFTS/XPS characterizations and analyzed the data. A.C. synthesized the HGaAlMFI catalyst. J.H. supervised the DHA catalyst preparation. Z.X.

and J.G.C. performed and analyzed the *in situ* XAS/XRD measurements. M.E.H. and D.B. developed the process model and carried out the techno-economic and life-cycle analyses. L.N. contributed to the thermodynamic analysis and experimental design, and coordinated the TEA/LCA work. F.L., B.J., L.N. and I.S. wrote the manuscript with input from all authors.

Data availability

The data supporting the findings of this study are available within the article and its Supplementary Information. Source data for the figures are provided with this paper.

Competing Interests

This work was supported in part by the US Department of Energy (DE-FE0032507). The prime recipient of this support is Redox and Catalytic Solutions, LLC, an NC State University-based startup company with Fanxing Li and Luke Neal as co-founders.

References

1. Schwach, P., Pan, X. & Bao, X. Direct Conversion of Methane to Value-Added Chemicals over Heterogeneous Catalysts: Challenges and Prospects. *Chem. Rev.* **117**, 8497–8520 (2017).

2. Liu, Y., Deng, D. & Bao, X. Catalysis for Selected C1 Chemistry. *Chem* **6**, 2497–2514 (2020).

3. Zhang, J., Meerman, H., Benders, R. & Faaij, A. Comprehensive review of current natural gas liquefaction processes on technical and economic performance. *Applied Thermal Engineering* **166**, 114736 (2020).

4. Amini, H. R. & Reinhart, D. R. Regional prediction of long-term landfill gas to energy potential. *Waste Management* **31**, 2020–2026 (2011).

5. Kougias, P. G. & Angelidaki, I. Biogas and its opportunities—A review. *Front. Environ. Sci. Eng.* **12**, 14 (2018).

6. Mansoor, R. & Tahir, M. Recent Developments in Natural Gas Flaring Reduction and Reformation to Energy-Efficient Fuels: A Review. *Energy Fuels* **35**, 3675–3714 (2021).

7. Omobolanle, O. C. & Ikiensikimama, S. S. Gas flaring: technicalities, challenges, and the economic potentials. *Environ Sci Pollut Res* **31**, 40838–40850 (2024).

8. Olivos-Suarez, A. I. *et al.* Strategies for the Direct Catalytic Valorization of Methane Using Heterogeneous Catalysis: Challenges and Opportunities. *ACS Catal.* **6**, 2965–2981 (2016).

9. Blankenship, A., Artsiusheuski, M., Sushkevich, V. & van Bokhoven, J. A. Recent trends, current challenges and future prospects for syngas-free methane partial oxidation. *Nat Catal* **6**, 748–762 (2023).

10. Kiani, D., Sourav, S., Tang, Y., Baltrusaitis, J. & Wachs, I. E. Methane activation by ZSM-5-supported transition metal centers. *Chem. Soc. Rev.* **50**, 1251–1268 (2021).

11. Çağlayan, M. *et al.* Initial Carbon–Carbon Bond Formation during the Early Stages of Methane Dehydroaromatization. *Angewandte Chemie International Edition* **59**, 16741–16746 (2020).

12. Lee, J.-J., Lee, S., Bae, Y.-S., Lee, J. & Kim, Y. T. Non-oxidative direct conversion of methane: Improved reactivity via linkage with dehydroaromatization. *Fuel Processing Technology* **256**, 108067 (2024).

13. Caglayan, M. *et al.* Illuminating the intrinsic effect of water co-feeding on methane dehydroaromatization: a comprehensive study. *ACS Catalysis* **11**, 11671–11684 (2021).

14. Ma, S., Guo, X., Zhao, L., Scott, S. & Bao, X. Recent progress in methane dehydroaromatization: From laboratory curiosities to promising technology. *Journal of Energy Chemistry* **22**, 1–20 (2013).

15. Kosinov, N. & Hensen, E. J. M. Reactivity, Selectivity, and Stability of Zeolite-Based Catalysts for Methane Dehydroaromatization. *Advanced Materials* **32**, 2002565 (2020).

16. Hensen, E. J. *et al.* In situ Ga K edge XANES study of the activation of Ga/ZSM-5 prepared by chemical vapor deposition of trimethylgallium. *Catalysis Letters* **101**, 79–85 (2005).

17. Cao, Z. *et al.* Natural Gas to Fuels and Chemicals: Improved Methane Aromatization in an Oxygen-Permeable Membrane Reactor. *Angew. Chem. Int. Ed.* **52**, 13794–13797 (2013).

18. Morejudo, S. H. *et al.* Direct conversion of methane to aromatics in a catalytic co-ionic membrane reactor. *Science* **353**, 563–566 (2016).

19. Brady, C., Murphy, B. & Xu, B. Enhanced methane dehydroaromatization via coupling with chemical looping. *ACS Catal.* **7**, 3924–3928 (2017).

20. Brady, C. *et al.* An integrated methane dehydroaromatization and chemical looping process. *Chemical Engineering Journal* **406**, 127168 (2021).

21. Kumar, A., Song, K., Liu, L., Han, Y. & Bhan, A. Absorptive hydrogen scavenging for enhanced aromatics yield during non-oxidative methane dehydroaromatization on Mo/H-ZSM-5 catalysts. *Angewandte Chemie International Edition* **57**, 15577–15582 (2018).

22. Haki, M., Linke, P., Costa, I. M. & Al-Rawashdeh, M. Methane conversion to aromatics via chemical synergy with OCM: Effect of periodic operation, temperature profile, and catalyst loading. *Fuel Processing Technology* **270**, 108189 (2025).

23. Zhao, K. *et al.* Lithium carbonate-promoted mixed rare earth oxides as a generalized strategy for oxidative coupling of methane with exceptional yields. *Nat Commun* **14**, 7749 (2023).

24. Zhou, Y. *et al.* Ethylene Dehydroaromatization over Ga-ZSM-5 Catalysts: Nature and Role of Gallium Speciation. *Angewandte Chemie International Edition* **59**, 19592–19601 (2020).

25. Brody, L. *et al.* Synergistic Cooperation of Dual-Phase Redox Catalysts in Chemical Looping Oxidative Coupling of Methane. *ACS Catal.* **14**, 13112–13125 (2024).

26. Cheng, Z. *et al.* C2 Selectivity Enhancement in Chemical Looping Oxidative Coupling of Methane over a Mg–Mn Composite Oxygen Carrier by Li-Doping-Induced Oxygen Vacancies. *ACS Energy Lett.* **3**, 1730–1736 (2018).

27. Wang, J., Liu, F., Wu, J., Zou, S. & Fan, J. Low-temperature oxidative coupling of methane over LaCeZr ternary oxide supported Mn–Na2WO4. *Catal. Sci. Technol.* **13**, 2493–2499 (2023).

28. Kazansky, V. B., Subbotina, I. R., van Santen, R. A. & Hensen, E. J. M. DRIFTS study of the nature and chemical reactivity of gallium ions in Ga/ZSM-5: II. Oxidation of reduced Ga species in ZSM-5 by nitrous oxide or water. *Journal of Catalysis* **233**, 351–358 (2005).

29. Mehdad, A., Gould, N. S., Xu, B. & Lobo, R. F. Effect of steam and CO2 on ethane activation over Zn-ZSM-5. *Catalysis Science & Technology* **8**, 358–366 (2018).

30. Phadke, N. M. *et al.* Characterization of isolated Ga3+ cations in Ga/H-MFI prepared by vapor-phase exchange of H-MFI zeolite with GaCl3. *ACS Catalysis* **8**, 6106–6126 (2018).

31. Meng, X. *et al.* Influence of different Ga species in MWW zeolite bifunctional catalysts on the ethane dehydrogenation and dehydroaromatization in the absence and presence of CO2. *Fuel* **363**, 130968 (2024).

32. Surdu-Bob, C. C., Saied, S. O. & Sullivan, J. L. An X-ray photoelectron spectroscopy study of the oxides of GaAs. *Applied Surface Science* **183**, 126–136 (2001).

33. Kazansky, V. B., Subbotina, I. R., Van Santen, R. A. & Hensen, E. J. M. DRIFTS study of the chemical state of modifying gallium ions in reduced Ga/ZSM-5 prepared by impregnation: I. Observation of gallium hydrides and application of CO adsorption as a molecular probe for reduced gallium ions. *Journal of Catalysis* **227**, 263–269 (2004).

34. Schreiber, M. W. *et al.* Lewis–Brønsted acid pairs in Ga/H-ZSM-5 to catalyze dehydrogenation of light alkanes. *Journal of the American Chemical Society* **140**, 4849–4859 (2018).

35. Garg, S., Xie, Z., Lam, A. X. & Chen, J. G. Tandem Electrocatalytic–Thermocatalytic Conversion of CO2 to Aromatic Hydrocarbons. *ACS Energy Lett.* **9**, 2990–2996 (2024).

36. Gomez, E., Nie, X., Lee, J. H., Xie, Z. & Chen, J. G. Tandem Reactions of CO2 Reduction and Ethane Aromatization. *Journal of the American Chemical Society* **141**, 17771–17782 (2019).

37. Gusev, A. A., Psarras, A. C., Triantafyllidis, K. S., Lappas, A. A. & Diddams, P. A. Effect of steam deactivation severity of ZSM-5 additives on LPG olefins production in the FCC process. *Molecules* **22**, 1784 (2017).

38. Wei, Z. *et al.* Steamed Zn/ZSM-5 catalysts for improved methanol aromatization with high stability. *Fuel Processing Technology* **162**, 66–77 (2017).

39. Skone, T. J. *et al. Carbon Dioxide Utilization Life Cycle Analysis Guidance for the U.S. DOE Office of Fossil Energy.* (2019).

40. Clariant, CATOFIN propane dehydrogenation. https://www.clariant.com/en/Business-Units/Catalysts/Petrochemical-and-Refining-Catalysts/CATOFIN-Technology. (Accessed 7/27/2026).

41. Won, W., Lee, K. S., Lee, S. & Jung, C. Repetitive control and online optimization of Catofin propane process. *Computers & Chemical Engineering* **34**, 508–517 (2010).

42. Nijhuis, T. A., Tinnemans, S. J., Visser, T. & Weckhuysen, B. M. Towards real-time spectroscopic process control for the dehydrogenation of propane over supported chromium oxide catalysts. *Chemical Engineering Science* **59**, 5487–5492 (2004).

43. Yang, H., Li, J. & Liu, Z.-W. Process validation of propane dehydrogenation in a CFB reactor with heat supply and catalyst regeneration: CFD simulation coupled with reaction kinetics. *Chemical Engineering Science* **313**, 121756 (2025).

44. Zhu, X., Imtiaz, Q., Donat, F., Müller, C. R. & Li, F. Chemical looping beyond combustion – a perspective. *Energy Environ. Sci.* **13**, 772–804 (2020).

45. Zou, S. *et al.* Selective oxidative coupling of methane via surface-confined methyl-radical transformation. Preprint at https://doi.org/10.26434/chemrxiv-2024-rmvt4 (2024).

46. Ravel, B. & Newville, M. ATHENA, ARTEMIS, HEPHAESTUS: data analysis for X-ray absorption spectroscopy using IFEFFIT. *J Synchrotron Rad* **12**, 537–541 (2005).

Methods

Catalyst preparation

$LaPrO_x@Li_2CO_3$ was prepared by using the modified Pechini method described in our previous work.[23] $La(NO_3)_3 \cdot 6H_2O$ (99.0%, Sigma-Aldrich) and $Pr(NO_3)_3 \cdot 6H_2O$ (99.0%, Sigma-Aldrich) were used as precursors and dissolved in deionized water, and citric acid (99.5%, Sigma-Aldrich) and ethylene glycol (99.8%, Sigma-Aldrich) were added into the solutions. The solution was stirred at 80 °C to form the gel. The gel precursor underwent 130 °C drying in an oven overnight and 950 °C calcination in air in a tube furnace for 10 h, labeled as $LaPrO_x$. The deposition of Li_2CO_3 ($\geq$ 99.0%, Sigma-Aldrich) onto $LaPrO_x$ was carried out by the wet impregnation method. The $LaPrO_x$ powder was soaked in the aqueous solution with a calculated amount of Li_2CO_3 and dried under stirring at 80 °C. The precursor further underwent 130 °C drying in an oven overnight and 750 °C calcination in a tube furnace for 3 h, giving the sample labeled $LaPrO_x@Li_2CO_3$.

Li-and B-promoted Mn–Mg-based redox oxide, $MnLi_aMg_bB_cO_x$ (MLMB), was prepared by milling the starting materials together in a planetary ball mill (XBM4X, Columbia International) as mentioned elsewhere.[25] Briefly, manganese dioxide (99.9%, Materion, 32.2 g), magnesia (99.9%, Materion, 42.3 g), boric acid (99.5%, Sigma-Aldrich, 11.3 g), and lithium hydroxide (98%, Sigma-Aldrich, 9.2 g) were mixed with water and ball milled for two hours. After milling, the slurry mixture was dried in an oven at 80 °C. The dried solid was then calcined in the muffle furnace in two steps with a heating ramp of 5 °C/min. It was first held at 450 °C for 3 hours and then at 900 °C for 8 hours.

$NaZrWO_x$ was prepared by a co-precipitation method.[45] In typical synthesis, tungsten hexachloride (99%, Fisher Scientific) and zirconium butoxide (80%, Sigma-Aldrich) were dissolved in ethanol at a W:Zr molar ratio of 1:3 under vigorous stirring to obtain a clear homogeneous solution. An aqueous solution of sodium hydroxide was then added dropwise to

make the precipitates, and the resulting mixture was kept stirring continuously for 3 h. The mixture was transferred to a petri dish and dried overnight at 40 °C, followed by further drying in an oven at 85 °C for 6 h. The dried solid was subsequently calcined in a muffle furnace at 850 °C with a heating ramp of 5 °C/min. In the MLMB-$NaZrWO_x$ composite, MLMB provides the primary CL-OCM function and $NaZrWO_x$ acts as a physically mixed promoter phase.

The HGaAlMFI catalyst was prepared following the conventional hydrothermal procedure for zeolite synthesis (with molar ratio of 5.25 TPAOH : 1.25 Na_2O : 25 SiO_2 : 0.63 Al_2O_3 : 0.41 Ga_2O_3 : 1000 H_2O), except that crystallization was performed under microwave heating. First, the HGaAlMFI zeolite precursor solution was prepared and stirred for 24 h, using deionized (DI) water, sodium hydroxide (NaOH), tetra-n-propylammonium hydroxide (TPAOH), tetraethyl orthosilicate (TEOS), sodium aluminate ($NaAlO_2$), and gallium nitrate hydrate ($Ga(NO_3)_3 \cdot {}_xH_2O$), all from Alfa Aesar. Following the solution preparation, they were placed into the Teflon-lined CEM MARs 6 Microwaves Easy Prep vessels with a stir bar. The solution was then ramped to 220 °C and held for 30 min. The resulting solution was then centrifuged and washed using DI water to separate out the resultant precipitate. This sample was then dried, calcined in flowing dry air (100 mL/min) at 550 °C for 5 h (1 °C/min ramp), and treated with a very similar process to the conventional method to obtain final HGaAlMFI catalyst. ICP-OES analysis of the elemental composition is provided in Table S29.

Reaction Testing

CL-OCM reaction

CL-OCM reaction test was conducted in a fixed bed U-tube quartz reactor with catalyst inside a 1/8-inch inner diameter. For a general test, 2.0 g of $LaPrO_x$@Li_2CO_3 (40-60 mesh) or 0.43 g of MLMB was loaded in the U-tube reactor, and inert aluminum grit was used to fix the catalyst bed. For the composite experiments, 0.215 g of $NaZrWO_x$ promoter was combined with 0.43 g of MLMB. A furnace was used to provide heat and control the temperature where the furnace

temperature was taken as the reaction temperature. For reaction step in CL-OCM reaction, 25 mL/min 80%CH_4/20%Ar was fed into the reactor for 15 s to 5 min. The non-condensable gas was collected in a gas bag and analyzed by gas chromatography (Agilent 7890B). Then Ar was fed into the reactor to flush the reaction. For the oxidation step, 25 mL/min 20%O_2/80%Ar was fed into the reactor, which was then followed by another Ar flush.

DHA reaction

DHA reaction test was conducted in a fixed bed U-tube quartz reactor with catalyst inside a 1/8-inch inner diameter. For a general test, 0.1 g HGaAlMFI (40-60 mesh) was loaded in the U-tube reactor and inert aluminum grit was used to fix the catalyst bed. A furnace was used to provide heat and control the temperature where the furnace temperature was taken as the reaction temperature. For the DHA reaction, C_2H_4 or C_2H_6 with Ar as balance was fed into the reactor. The product stream undergoes a cold trap with dodecane inside an impinger and ice water cooling. The gas product was collected with a gas bag and then analyzed by an Agilent 7890B GC. The liquid product was trapped in the dodecane, and the products-containing dodecane mixture was analyzed by an Agilent 7890A GC.

OCM+DHA tandem reaction

Tandem OCM+DHA reaction test was conducted in two fixed-bed U-tube quartz reactors with catalyst inside a 1/8-inch inner diameter. For a general test, the respective CL-OCM catalysts were loaded in the first U-tube reactor with inert aluminum grit to fix the catalyst bed, and the DHA catalyst was loaded in the second U-tube reactor with inert aluminum grit to fix the catalyst bed. Two furnaces were used to provide heat and control the temperatures, and the furnace temperature was taken as the reaction temperature. For the reaction step in the tandem OCM+DHA reaction, 25 mL/min 80%CH_4/20%Ar was fed into the first reactor for 15 s to 5 min. The effluent of the tandem reactor was passed through an impinger containing dodecane, cooled in an ice-water bath, to trap condensable aromatics. The non-condensable gas was

collected in a gas bag and analyzed by gas chromatography (Agilent 7890B). The dodecane solution was analyzed by gas chromatography (Agilent 7890A), and the aromatics were quantified using dodecane as an internal standard and converted to carbon moles; naphthalenes, which condense in the impinger and are not detected in the gas bag, were included in the total aromatics. Both reactors were then flushed with 25 mL/min Ar. For the regeneration step, 25 mL/min 20%O_2/80%Ar was fed to the OCM reactor and 25 mL/min 20%H_2/80%Ar to the DHA reactor (for the O_2-only regeneration of Fig. 2a, 20%O_2/80%Ar was fed to both reactors), followed by another Ar flush. Step durations for each experiment are listed in Table S1. The performance parameters are defined as below:

$$\text{Methane conversion } (X_{CH_4}) = \frac{\sum n_{C,\text{products}}}{\sum n_{C,\text{products}} + n_{C,CH_4,\text{out}}} \times 100\%$$

$$\text{Carbon selectivity to product i } (S_i) = \frac{n_{C,i}}{\sum n_{C,\text{products}}} \times 100\%$$

$$\text{Aromatic carbon yield} = X_{CH_4} \times \frac{S_{\text{aromatics}}}{100}$$

$$\text{Ethylene fraction} = \frac{n_{C,C_2H_4}}{n_{C,C_2H_4} + n_{C,C_2H_6}} \times 100\%$$

$$\text{Carbon Balance} = \frac{\sum n_{C,\text{products}} + n_{C,CH_4,\text{out}}}{n_{C,CH_4,\text{fed}}} \times 100\%$$

Catalyst characterizations

***In situ* X-ray absorption spectroscopy (XAS) and X-ray diffraction (XRD) measurements**

The combined in situ Ga K-edge XAS and time-resolved XRD measurements were carried out at beamline 7-BM (QAS, 10^{12} ph/s @ 10 keV) of the National Synchrotron Light Source II (NSLS-II) at Brookhaven National Laboratory (BNL). Since metallic Ga is liquid at around room temperature, the Ga K-edge XAS energy was calibrated using the Re foil L3-edge (10,535 eV), while the XRD incident X-ray energy was fixed and calibrated against the Mo foil K-edge (20,000 eV), corresponding to a wavelength of 0.6199 Å. To carry out the

combined in situ XAS-XRD measurements, a Clausen cell equipped with a quartz capillary (1.2 mm O.D., 1.0 mm I.D.) was utilized. For XRD, the sample-to-detector distance was calibrated using a CeO_2 standard. Fresh sample (60-80 mesh) was loaded into the quartz capillary and fixed between two pieces of quartz wool for each experiment. Two pretreatment-reaction conditions were employed: 1) Pretreatment in N_2 (20 mL min^{-1}) from room temperature to 550 °C at a heating ramp rate of 10 °C/min, held for 5 min, followed by C_2H_4/N_2 reaction (8/12 mL min^{-1}, 5 min), H_2 reduction (H_2/N_2 = 4/16 mL min^{-1}, 20 min), and another C_2H_4/N_2 reaction (8/12 mL min^{-1}, 5 min) at 550 °C. 2) Studies of steam effects involved passing N_2 or reaction gas through a water-filled glass bubbler at room temperature before entering the reaction cell. Specifically, the fresh sample was first treated with wet N_2 (20 mL min^{-1}), heated from room temperature to 550 °C at 10 °C/min, held for 5 min, then exposed to wet reaction mixture (C_2H_4/N_2 = 8/12 mL min^{-1}) at the same temperature for 5 min. Afterwards, the water bubbler was bypassed and only dry gases were fed into the cell. The sample was regenerated with H_2 (H_2/N_2 = 4/16 mL min^{-1}) at 550 °C for 20 min, after which the sample was tested under the reaction condition (C_2H_4/N_2 = 8/12 mL min^{-1}, 5 min). Throughout the process, the XAS spectrum and XRD pattern were collected alternately. For each collection cycle, XAS spectrum was firstly acquired utilizing both transmission and fluorescence modes, after which a two-dimensional (2D) diffraction image was captured using a Pilatus 1M area detector. The 2D images were processed and integrated using Dioptas software to obtain XRD profiles after subtracting the background. Ga_2O_3 served as an X-ray absorption near edge structure (XANES) reference for comparison with the catalysts and for determining the amplitude reduction factor ($S0^2$) for the extended X-ray absorption fine structure (EXAFS) fitting. All XAS data processing was performed using the IFEFFIT package.[46]

Temperature-programmed surface reaction (C_2H_4-TPSR)

C_2H_4-TPSR was performed on 30 mg of HGaAlMFI. To simulate water poisoning, the catalyst was first treated in steam at 550 °C for 1 h (5 mL/min H_2O(g) in 20 mL/min Ar). Water injection was then stopped, and the catalyst was reduced in 5 mL/min H_2 and 20 mL/min Ar at 550 °C for 1 h. The sample was cooled to 100 °C and flushed with Ar for 1 h. The TPSR was then run from 100 to 700 °C at 10 °C/min in a flow of 10% C_2H_4 in Ar (25 mL/min total), and the C_2H_4 signal was followed by mass spectrometry m/z = 26. The fresh catalyst was measured with the same procedure, omitting the steam treatment.

Temperature-programmed reduction (H_2-TPR)

H_2-TPR was performed on 30 mg of fresh or steam-treated HGaAlMFI. The steam-treated sample was first exposed to steam at 550 °C for 1 h (5 mL/min H_2O(g) in 20 mL/min Ar). Water injection was then stopped, and the sample was flushed with Ar at 550 °C, cooled to 100 °C and held in Ar for 1 h. The fresh sample received the same Ar treatment without steam. The sample was then heated from 100 °C at 10 °C/min in 10% H_2 in Ar (25 mL/min total), and H_2 consumption was monitored by mass spectrometry m/z = 2.

***Ex situ* X-ray photoelectron spectroscopy**

XPS was performed on a PHI 3057 spectrometer using an Al Kα X-ray source. Fresh and steam-treated HGaAlMFI samples were prepared as described for the C_2H_4-TPSR measurements and stored under Ar in a vial for analysis. Spectra were analyzed with CasaXPS software, and binding energies were calibrated to the adventitious C 1s peak at 284.8 eV.

***In situ* DRIFTS**

In situ DRIFTS experiments were carried out on a Nicolet IS50 spectrometer equipped with a Harrick Scientific DRIFTS cell with ZnSe windows. The *in situ* DRIFTS experiments were performed to record the evolution of surface species on HGaAlMFI during H_2 and steam treatments. Fresh catalyst (50 mg powdered sample) was loaded into the DRIFTS cell and flushed with Ar (50 mL/min) at 600 °C for 1 h to remove adsorbates. Background spectra

(resolution of 8 cm^{-1}, 64 scans) were then collected. Afterwards, the sample was treated with 42 vol% H_2/Ar (50 mL/min) at 300 °C or 550 °C for 1 h and then purged with Ar (50 mL/min) for 1 h. For the "H_2 and steam treatment" procedure, the catalyst was treated with H_2 at 550 °C followed by steam. The "steam and H_2 treatment" procedure proceeds through steam treatment first, followed by H_2 treatment at 550 °C. Steam was introduced as described for the C_2H_4-TPSR measurements. DRIFTS spectra were collected every 1 min.

Thermodynamic calculations

Equilibrium compositions and reaction enthalpies were calculated with HSC Chemistry 10 (version 10.6.3.0, Metso) using the Gibbs energy minimization module and its built-in thermodynamic database, treating the gas phase as an ideal mixture at 1 bar over 400–700 °C in 10 °C steps. The species considered were Ar, C_2H_4, C_2H_6, H_2O, H_2 and C_6H_6. Each case was set up on a basis of 100 kmol CH_4 fed to the oxidative coupling (OCM) step. Unconverted CH_4 was treated as inert and represented by an equal amount of Ar. The OCM step was assumed to convert the specified fraction of CH_4 exclusively to C_2H_4, C_2H_6 and H_2O, so that the DHA-step feed consisted of these C_2 products, H_2O and Ar. The aromatic yield was defined on a carbon basis and, for the 100 kmol CH_4 basis, equals (in %) 6 × the equilibrium kmol of C_6H_6. HSC reports the enthalpy change for the aromatization step only ($C_2H_4/C_2H_6 \rightarrow C_6H_6 + H_2$). The enthalpy of the OCM step ($CH_4 + O_2 \rightarrow C_2H_4/C_2H_6 + H_2O$) was calculated by Hess's law from HSC species enthalpies at each temperature. It was calculated separately for the ethylene route ($CH_4 + 1/2O_2 \rightarrow 1/2C_2H_4 + H_2O$) and the ethane route ($CH_4 + 1/4O_2 \rightarrow 1/2C_2H_6 + 1/2H_2O$), weighted by the C_2H_4:C_2H_6 ratio, and scaled by the conversion. Because the HSC feed was entered at 25 °C, the exported enthalpy also contains the sensible heating of the inert Ar from 25 °C to T. This was subtracted so that the reported values approximate isothermal heats of reaction. The corrected aromatization enthalpy and the OCM enthalpy were summed and

normalized by the CH_4 feed, giving the net ΔH in kJ per mol CH_4 fed. At zero conversion no reaction occurs, so ΔH was set to zero.

Process Modeling, Techno-Economic and Life Cycle Analyses

Aspen Plus v14 was used to develop a process model for converting natural gas (NG) into value-added organic liquids—via an integrated Oxidative Coupling of Methane and Dehydroaromatization (OCM-DHA) process. The model considers benzene, toluene, xylene, and naphthalene as the primary products based on experimental data, either as individual products separated on-site or as a non-separated organic liquid. In addition to a baseline system that does not mitigate CO_2 emissions, the system accounts for generated carbon dioxide (CO_2) through two cases:

Capture: 80–90% of the generated CO_2 is captured using an amine-based system (e.g., Cansolv solvent). The remaining CO_2, along with other unreacted components, is recycled within the process.

Methanation: The produced CO_2 undergoes methanation, where 90% is converted to CH_4 and recycled.

Modeling was further subdivided to address two technoeconomic scenarios:

Complete Separation: Major products (Benzene, toluene, xylene, and naphthalene) are separated on site using distillation columns.

Py Gas: The liquid hydrocarbon product is exported as a Pyrolysis Gasoline type mixture.

Initial modeling assumes a plant capacity of 50 bbl/day of organic liquids, aligning with the expected capacity at “stranded” natural gas sites. To avoid the build-up of inert or unconverted gases, a purge stream is incorporated in both cases.

Extensive descriptions of the process model, as well as techno-economic and life cycle analysis calculations are provided in the SI.

A life cycle assessment (LCA) is also conducted to evaluate the greenhouse gas (GHG) emissions associated with the OCM-DHA process to assess its environmental impact to inform future investment decisions and technology adoption strategies. The same modeling cases from the TEA were used for these analyses. Life cycle inventories (LCIs) for each case were developed using SimaPro v9.6.01, utilizing unit process data primarily from the Ecoinvent 3 database. Environmental impact characterization was performed using the TRACI 2.1 method developed by the U.S. Environmental Protection Agency (EPA); however, this analysis focused exclusively on global warming potential (GWP), represented by greenhouse gas (GHG) emissions. A detailed description of the LCA is provided in the SI.

Supplementary Files

This is a list of supplementary files associated with this preprint. Click to download.

- OCMDHASI10282026Final.docx